Electronic structure of Indium-Tungsten-Oxide alloys and their energy band alignment at the heterojunction to crystalline silicon

Dorothee Menzel,[1, a)] Mathias Mews,[1] Bernd Rech,[1] and Lars Korte[1]
Helmholtz-Zentrum Berlin, Institute of Silicon Photovoltaics, Kekuléstraße 5, D-12489 Berlin, Germany

The electronic structure of thermally co-evaporated indium-tungsten-oxide films is investigated. The stoichiometry is varied from pure tungsten oxide to pure indium oxide and the band alignment at the indium-tungsten-oxide/crystalline silicon heterointerface is monitored. Using in-system photoelectron spectroscopy, optical spectroscopy and surface photovoltage measurements we show that the work function of indium-tungsten-oxide continuously decreases from 6.3 eV for tungsten oxide to 4.3 eV for indium oxide, with a concomitant decrease of the band bending at the hetero interface to crystalline silicon than indium oxide.

Metal oxide layers have found a plethora of applications within different electronic devices. They are used as transparent conductive layers in optoelectronic devices such as flat-panel displays and solar cells, as electron and hole extracting contacts in many solar cell technologies such as perovskite[1], silicon heterojunction[2,3], chalcopyrite[4] and organic molecule based solar cells[5], as well as in light emitting devices[6]. Additionally they are used as passivation layers and dielectrics in CMOS[7] and in electrochromic devices[8].

Two of the most commonly used metal oxides are indium(III)-oxide (In_2O_3) and tungsten(VI)-oxide (WO_3). Indium oxide (InO_x) is most commonly doped with tin and used as n-type transparent conductive oxide in flat-panel displays and solar cells. Alternative dopants like hydrogen[9], molybdenum[10], zinc[9] and tungsten[11] have been applied and yielded high carrier mobilities, which in turn enabled higher conductivities, or lower free carrier absorption at similar conductivities compared to indium-tin-oxide (ITO). Indeed, the characteristic advantage of InO_x is its comparatively high conductivity with a variety of different dopants. At typical doping levels InO_x is degenerately doped and has a work function of about 4.7 eV[12], which is below the level required to properly contact the valence band, or highest occupied molecular orbital, of typical semiconductors like crystalline silicon (c-Si) (at 5.12 eV[13]), $Cu(In,Ga)(S,Se)_2$ (at about 5.5 eV[14]), amorphous silicon (at 5.4 eV[15]), $CH_3NH_3PbI_3$ (at 5.4 eV[16]) and anthracene (at 5.75 eV[17]). Indeed, for application in silicon heterojunction solar cells, this has been identified as limiting factor[18].

Tungsten oxide (WO_x) is most widely used as an electrochromic layer[8]. Additionally its valence band position is below the water oxidation energy, which has led to investigations of WO_x as water oxidiser in water splitting devices[19,20]. Furthermore its high work function (about 5.5 to 6.5 eV[21]) and good thermal stability[22] have led to applications as hole extraction layers in silicon heterojunction[18,23], crystalline silicon[24], perovskite[1] and organic molecule based solar cells[25], and in light-emitting devices[6]. However, the low conductivity of high work function WO_x has proven problematic[18,26,27]. Furthermore, it is prone to the generation of oxygen vacancy defects, which reduce its work function[26] and transparency[1].

Overall these two materials are complementary regarding the applications as a hole contact on typical semiconductors and as an electrode for water oxidation. The work function of WO_x is more than adequate to contact the valence bands of silicon, $Cu(In,Ga)(S,Se)_2$, or perovskite and to oxidize water, but its conductivity needs to be improved. Contrary to this, InO_x has a sufficiently high conductivity, but features a work function that is insufficient to contact the valence bands of the mentioned materials.

The consequential idea is to combine both materials and search for a trade-off. There are reports on indium-tungsten-oxide (IWO_x) layers with up to 7 % WO_x applied as transparent conductive oxides[11,28]. These layers are among the doped InO_x layers with the highest mobility[11]. Furthermore WO_x doped InO_x films (1 wt%) have been applied in silicon heterojunction solar cells as double anti reflective coating leading to up to 23 % efficiency[29]. However, there is no systematic study investigating the full range of IWO_x from pure WO_x to pure InO_x. The purpose of the present study is to investigate the electronic structure of IWO_x alloys ranging in composition from pure In_2O_3 to pure WO_3 using photoelectron spectroscopy and optical spectroscopy.

200 μm thick, phosphorous doped n-type (1-2 Ωcm) crystalline silicon (c-Si) wafers were used as substrates. The wafers were cleaned using the RCA cleaning process. To remove the native silicon oxide on the surface, the wafers were dipped in 1 % HF for 2 min and transferred into vacuum. Samples were prepared and measured under ultra high vacuum conditions (10^{-9} mbar base pressure) without breaking the vacuum inbetween deposition and photoelectron spectroscopy measurements. In_2O_3 (99.994 %) and WO_3 (99.99 %) were deposited by thermal co-evaporation using an aluminium oxide boat and a tungsten crucible, respectively. During deposition the wafer was rotated with 1.3 rotations per second. The ratio between deposited In_2O_3 and WO_3 was varied by changing the crucible temperatures

a)Electronic mail: dorothee.menzel@helmholtz-berlin.de

from 920 °C to 1020 °C for WO_3 and from 1260 °C to 1350 °C for In_2O_3, yielding deposition rates from about 0.4 to 5 nm/min and about 10 nm thick layers. The substrate was not intentionally heated and is about 20 cm away from the crucibles. Therefore no significant heating of the substrate during evaporation is expected. However an impact on the oxygen vacancy density in the deposited metal oxides by the different crucible temperatures cannot be excluded. For this study the impact is neglected, since the crucible temperature range is small and therefore the effect should be negligible[30].

Thermal evaporation was applied in this study, since co-evaporation enables easy variations of the indium to tungsten ratio in the metal oxide alloy, without necessitating distinct changes of the deposition conditions. Apart from thermal evaporation[31,32] In_2O_3 and WO_3 can be deposited using magnetron sputtering[10,33], atomic layer deposition[34,35], or chemical vapor deposition[36,37]. Depending on the applied deposition method the electronic structure i.e. the amount of oxygen vacancies[26], the crystalline structure[33] and the density of precursor residues and contaminations[34] in the metal oxide can be affected. Instead of thermal co-evaporation, as performed in this study, also other co-deposition techniques, such as co-sputtering[28] are commonly used.

X-ray photoelectron spectroscopy (XPS) with Al-K_α excitation was used to investigate the In to W ratio of the metal oxide alloy. The XPS analysis was conducted using the W 4f, In 3d and O 1s core levels. The In and W contents of the metal oxides were calculated using sensitivity factors extracted from fully stoichiometric WO_3 and In_2O_3 samples, which have been oxidized by an oxygen plasma at 10^{-5} mbar for 10 min. The ratio of the metal oxide peak area to the O 1s peak area, corrected by the stoichiometry of the respective element was used as sensitivity factor. These sensitivity factors were used to obtain the fraction of InO_x in the mixture of InO_x and WO_x.

Afterwards the core levels were analysed in more detail. A Shirley background was assumed for all spectra. The In $3d_{3/2}$ core level was fitted with the following four signals: First oxidic indium (In^{3+}), second metallic indium (In(met.)) with an energy separation of 1.2 eV towards lower binding energy[38], third indium hydroxide ($In(OH)_3$) with a 0.9 eV higher binding energy[39] and a loss feature at about 2.7 eV higher binding energy compared to In^{3+}.

The model for the W 4f orbital consists of a doublet of the 7/2 and 5/2 spin states with an energy separation of 2.12 eV between the two components of the doublet, an area ratio of 3/4 and the same full width at half maximum for both peaks. In this experiment we observe W^{6+} and W^{5+} with a separation of 1.2 eV between the respective oxidation states[40,41].

Helium ultra-violet photoelectron spectroscopy (He-UPS) was applied to investigate the work function (WF) and valence band edge position (E_V-E_F) of the metal oxides. The secondary electron cut-off was measured and fitted using a Boltzmann-Sigmoid function to obtain the work function of the layers. Additionally (E_V-E_F) was extracted from the He-UPS spectra using a linear fit to the leading edge of the spectrum. Layer thicknesses were determined from spectral ellipsometry data in a wavelength range of 190 to 850 nm using a model with a combination of a Drude-Lorentz and a Tauc-Lorentz[42] oscillator. For layers with more than 50 % indium oxide the Drude-Lorentz oscillator was mostly sufficient for the fitting and the area of the Tauc-Lorentz was negligible[43], whereas for layers with more than 50 % WO_x the amplitude of the Drude-Lorentz was negligible and the Tauc-Lorentz was sufficient for data fitting[44]. The band gaps of the layers were extracted using transmission and reflection measurements obtained from about 50 nm thick IWO_x layers on glass in the wavelength range of 250-1500 nm. A Tauc-gap[45] with an energy dependence of $(h\nu\alpha)^{1/2}$ was assumed to determine the band gap, where the exponent corresponds to an allowed indirect band transition[46]. Surface photo voltage (SPV) measurements with 905 nm laser excitation[47] were carried out on samples with IWO_x on n-type c-Si. These measurements allow to quantify the c-Si band bending at the interface to the IWO_x film.

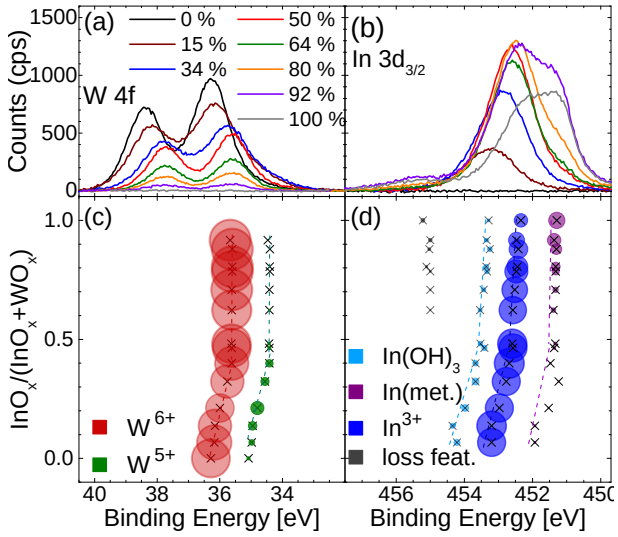

FIG. 1. Background-corrected XPS spectra of the (a) W 4f and (b) In $3d_{3/2}$ core levels for 8 samples starting from pure InO_x (grey, 100 % indium) to pure WO_x (black, 0 % In). The legend shows the fraction of InO_x in the IWO_x. The results of the analysis of the (c) W $4f_{7/2}$ and (d) In $3d_{3/2}$ core levels are shown, where the InO_x fraction corresponds to the vertical and the binding energy to the horizontal axis. The symbol area represents the relative area of the individual peaks compared to the entire core level intensity.

Fig. 1 shows a selection of XPS measurements of the W 4f (panel a) and In $3d_{3/2}$ (panel b) core levels collected from samples with different InO_x and WO_x contents. It is obvious that samples with a high W 4f signal intensity show low intensities for In $3d_{3/2}$ and vice versa. For both signals a shift towards lower binding

energies with increasing InO_x content is observed. This data in combination with the sensitivity factors is used to calculate the InO_x and WO_x content of each sample. In addition, the results of the peak fitting analysis of the W 4f and the In $3d_{3/2}$ core levels are depicted in panels c and d, respectively. Evaluating the W 4f core level, we observe that the binding energy decreases linearly by about 700 meV with increasing InO_x content from pure WO_x up to 50 % InO_x content. For an InO_x content higher than 50 % the binding energy stays constant. Considering the relative intensity of the different oxidation states, we observe solely W^{6+} for an InO_x content higher than 50 %, which corresponds to stoichiometric tungsten trioxide, WO_3. For an InO_x content of less than 50 %, also W^{5+} can be observed with a relative amount of 8 % to 32 %, which indicates the presence of oxygen deficient WO_x in tungsten rich layers. For the In 3d core level (panel d) we observe almost the same shift in binding energy as in the W 4f core level. The binding energy decreases linearly with increasing InO_x content up to 50 % InO_x content and decreases only slightly with InO_x content higher than 50 %. Up to 80 % InO_x content the oxidic indium (In^{3+}) dominates the core level signal intensity, while indium hydroxide accounts for 10 % to 15 % relative intensity. For higher InO_x content than 80 %, metallic indium gains a high relative proportion of the peak intensity, up to 45 % of the total signal intensity, and a loss feature at higher binding energy is observed. Since these two signals are loosely correlated, it is possible that the loss feature is related to plasmons of the metallic indium.

We continue with analysing the electronic structure, especially work function (WF), (E_V-E_F), band gap (E_G) and the band bending (ϕ) in the metal oxide/silicon-junction. The measured WF values are shown in Fig. 2a, the band bending from SPV is shown in Fig. 2b and E_V-E_F and E_G values are shown in Fig. 2c. We can observe a strong decrease of the WF from 6.27 eV for pure WO_x to about 4.5 eV for an InO_x content of about 50 %. The work function remains almost constant for an InO_x content between 50 % and 80 %. We can observe a second, much less pronounced decrease in WF by about 0.2 eV for IWO_x with more than 80 % InO_x content. Finally, the WF of pure InO_x is about 4.24 eV. All in all the WF of the metal oxide mixture and the binding energies of the W 4f and In $3d_{3/2}$ core levels follow the same trend, but the change in WF is a lot more pronounced than the one seen for the core levels. Additionally the minor WF decrease for high InO_x contents coincides with the increasing signal of metallic indium and the rise of the loss feature in the In $3d_{3/2}$ orbital. Overall the work function changes by almost 2 eV for varying InO_x and WO_x content in the alloy. Furthermore, a small amount of InO_x in WO_x leads to a significant decrease in WF, whereas a small amount of WO_x in InO_x only slightly increases WF.

The band bending data (2b) shows pronounced fluctuations, but the same overall trend as the WF data. The total change in band bending from pure WO_x to pure InO_x is about 200 meV. This will be evaluated in more detail later in the discussion of the IWO_x/c-Si interface. Interestingly, the variations in the valence band position relative to E_F (Fig. 2c) are only 320 meV, i.e. of the same order of magnitude as the E_G variation, but much less pronounced than the variation in WF.

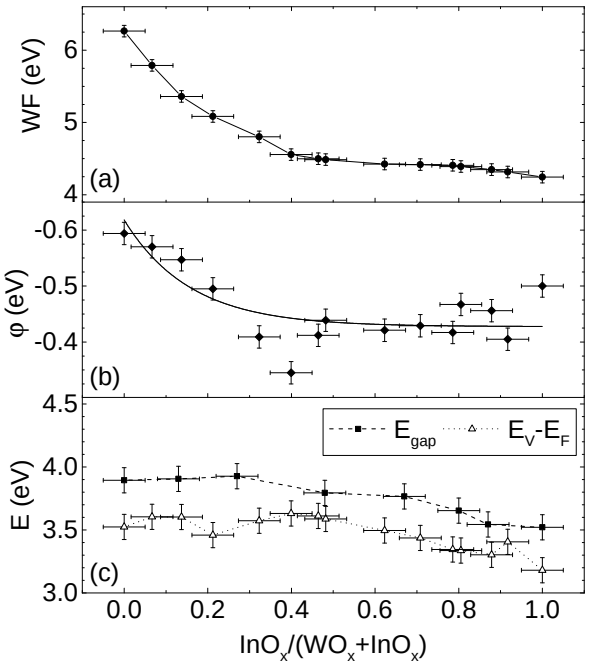

FIG. 2. (a) work function (WF) of IWO_x, (b) band bending (φ) in IWO_x/c-Si junctions and (c) valence band edge position (E_V-E_F) and band gap (E_G) of IWO_x layers plotted versus the fraction of InO_x in the IWO_x. The line in panel (b) is a guide to the eye.

Combining the above mentioned data leads to the band energy alignment vs. varying InO_x content as shown in Fig. 3, where all energy values are plotted relative to the Fermi level (E_F). The most pronounced change in the band alignment is the change in distance of E_F from the vacuum energy, i.e. the work function. As discussed above (Fig. 2a) the valence band edge as well as the band gap follow the same trend and decrease slightly by about 0.4 eV towards higher InO_x content. Hence, the energetic position of the conduction band stays constant at about +0.3 eV relative to E_F, whereas the valence band approaches the Fermi level from -3.5 eV for pure WO_x to -3.18 eV for pure InO_x. The finding of a fixed E_F-E_C ~0.3 eV is in line with previous findings[48].

Klein et al.[12] measured the work function of common transparent conductive oxides like ITO, aluminium doped zinc oxide and antimony doped tin oxide and related them to the valence band positions of these materials. Comparing these results to the work functions and valence band positions measured in this study, we find that WO_x offers higher work functions at the

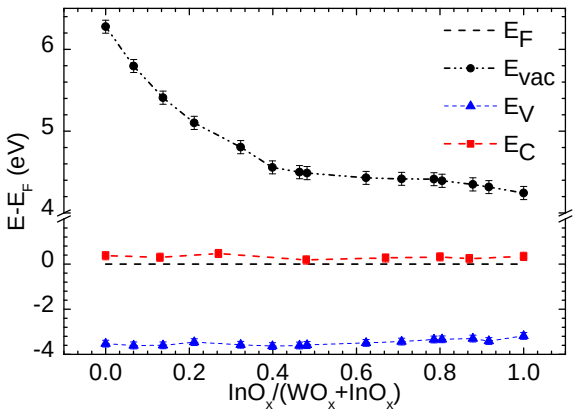

FIG. 3. Band alignment of IWO_x thin films on silicon plotted versus the InO_x content in IWO_x. The vacuum energy (E_{vac}), the valence (E_V) and conduction band edge (E_C) position are reported relative to the Fermi-level (E_F) and plotted versus the fraction of InO_x in the IWO_x alloy.

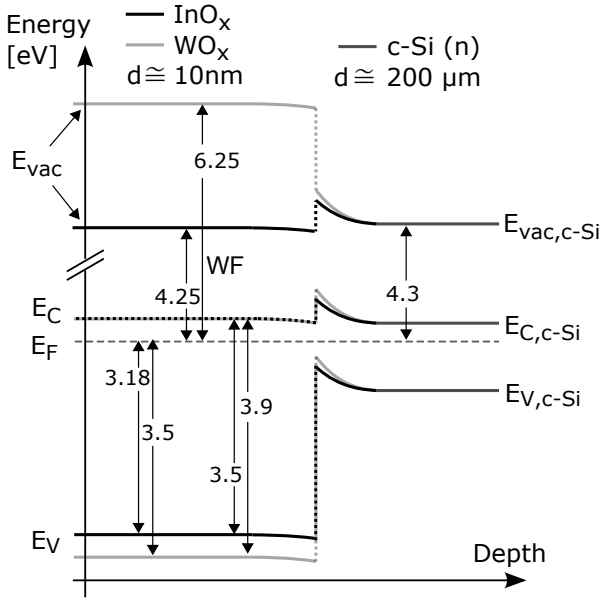

FIG. 4. Sketch of the heterojunction between WO_x (grey line)/ InO_x (black line) and n-type c-Si (dark grey line) with work function (WF), valence band edge (VB) and band gap (E_G). Values for WO_x and InO_x values obtained using He-UPS, optical spectroscopy and surface photovoltage and values for c-Si were taken from literature with a donor density of $10^{15}\mathrm{cm}^{-3}$.

same valence band positions achievable for ITO and tin-oxide. Indium doping of WO_x could thus enhance the electrical conductivity of WO_x based water oxidizers in photo-electrical water splitting devices[19], without elevating the valence band above the water oxidation level.

Using the additional information on c-Si band bending from 2b, we now discuss the heterojunctions of InO_x/c-Si (black line) and WO_x/c-Si (grey line) in Fig. 4. Crystalline silicon is assumed with a band gap of 1.12 eV, an electron affinity of 4 eV[13]. With the present dopant concentration this yields a WF of 4.3 eV. The band alignment at the IWO_x/c-Si contact is defined by the band bending in the c-Si as measured using SPV and the valence- and conduction band positions of the metal oxide layer as discussed above. Note, that we assume no band bending in the IWO_x film, i.e. a strong E_F pinning by the states at 0.3 eV below E_C

Due to the conduction band position of WO_x at 0.37 eV above E_F and the band bending at the interface of -0.59 eV there is an offset of $(E_C-E_F)_{WO_x}-(E_V-E_F)_{c-Si}-q\varphi = 0.58\,\mathrm{eV}$ between the conduction band of WO_x and the valence band of c-Si. It has been surmised that the conduction of carriers in these high work function metal oxides is facilitated by defect states close to E_F and the metal oxide conduction band[2,24]. The offset between the Fermi-level in WO_x and the valence band of c-Si is only 0.21 eV. This offset can easily be overcome by thermionic emission[49] and therefore enables a suitable recombination contact. However, a good selectivity for transport is only obtained, if a strong band bending is preventing electrons from reaching the interface[13,50]. The band bending of -0.59 eV should suffice to achieve this carrier selectivity.

Evaluating the InO_x/c-Si heterojunction, a lower band bending of about -0.44 eV is measured. This leads to an offset of about 0.73 eV between the InO_x conduction band and the c-Si valence band, or 0.36 eV between E_F in InO_x and the c-Si valence band. These bigger offsets should lead to a comparatively worse recombination contact at this interface, as compared to WO_x/c-Si, and the lower band bending should lead to less pronounced carrier selectivity.

Comparing the WF difference from pure WO_x to pure InO_x, we find that the overall change of the SPV band bending amounts to only 10 % of the overall change of the work function. SPV measurements are known to slightly underestimate the actual band bending[51]. Both, a higher band bending as well as a downwards band bending in the IWO_x film would reduce the band offset, so that the above mentioned values of the band offsets have to be seen as upper limits. Nevertheless, the significant deviation of the difference in WF and the measured band bending suggests that the non-passivated interface between c-Si and IWO_x leads to a high defect density and dipoles at the interface, which can also be seen in Fig. 4 with band offsets of more than 1.3 eV in vacuum energy. Comparing the offset in the vacuum energy levels at the InO_x/c-Si and WO_x/c-Si interface, even an inversion of the surface dipole charge is observed. The factor of about 0.1 between the actual band bending and the difference in work functions indicates that the naive Anderson model of calculating band offsets from WFs does not hold, in accordance with similar studies on other heterointerfaces. Similar factors have been reported due to Fermi-level pinning[52] in semiconductor-

heterojunctions, dipoles on silicon surfaces[53] and the defective interface in Schottky junctions[54]. Nonetheless, indium-tungsten-oxide's higher work function could prove useful for hole contacts to typical device relevant semiconductors used in microelectronics and photovoltaics, such as silicon and $Cu(In,Ga)(Se,S)_2$, or perovskites. However, the presence of interface defects and dipoles leads to a much less pronounced change of the band line up between c-Si and IWO_x with changing stoichiometry than expected. Further studies on the influence of SiO_x[55] and/or additional passivating interlayers at the interface, direct measurement of the band offset by surface inversion layer conductance measurements[56] or XPS valence band spectra[57] are suitable next steps towards a full understanding of this material system

ACKNOWLEDGEMENT

The authors would like to thank Thomas Lußky for vacuum system maintenance, Kerstin Jacob for wafer cleaning and Daniel Meza for the deposition of thick layers on glass. This project has received funding from the European Union's Horizon 2020 research and innovation programme under grant agreement No 727523 (NextBase).

[1] J. Werner, J. Geissbühler, A. Dabirian, S. Nicolay, M. Morales-Masis, S. De Wolf, B. Niesen, and C. Ballif, ACS Appl. Mater. Interfaces **8**, 17260 (2002).
[2] C. Battaglia, S. Martín de Nicolás, S. De Wolf, X. Yin, M. Zheng, C. Ballif, and A. Javey, Appl. Phys. Lett. **104**, 113902 (2014).
[3] J. Bullock, M. Hettick, J. Geissbühler, A. J. Ong, T. Allen, C. M. Sutter-Fella, T. Chen, H. Ota, E. W. Schaler, S. De Wolf, et al., Nat. Energy **2**, 15031 (2016).
[4] N. Naghavi, D. Abou-Ras, N. Allsop, N. Barreau, S. Bücheler, A. Ennaoui, C.-H. Fischer, C. Guillen, D. Hariskos, J. Herrero, et al., Prog. Photovolt: Res. Appl. **18**, 411 (2010), ISSN 1099-159X.
[5] M. T. Greiner, M. G. Helander, W.-M. Tang, Z.-B. Wang, J. Qiu, and Z.-H. Lu, Nat. Mater. **11**, 76 (2012).
[6] J. Meyer, T. Winkler, S. Hamwi, S. Schmale, H.-H. Johannes, T. Weimann, P. Hinze, W. Kowalsky, and T. Riedl, Adv. Mater. **20**, 3839 (2008).
[7] J. Robertson and R. M. Wallace, Mater. Sci. Eng. R-Rep. **88**, 1 (2015).
[8] C. G. Granqvist, Sol. Energ. Mat. Sol. Cells **60**, 201 (2000).
[9] N. Ito, Y. Sato, P. K. Song, A. Kaijio, K. Inoue, and Y. Shigesato, Thin Solid Films **496**, 99 (2006).
[10] Y. Yoshida, D. M. Wood, T. A. Gessert, and T. J. Coutts, Appl. Phys. Lett. **84**, 2097 (2004).
[11] Y. Abe, N. Ishiyama, H. Kuno, and K. Adachi, J. Mater. Sci. **40**, 1611 (2005).
[12] A. Klein, C. Körber, A. Wachau, F. Säuberlich, Y. Gassenbauer, S. P. Harvey, D. E. Proffit, and T. O. Mason, Materials **3**, 4892 (2010).
[13] S. M. Sze and K. K. Ng, *Physics of Semconductor Devices* (Wiley-Interscience, 2007).
[14] S.-H. Wei, S. B. Zhang, and A. Zunger, Appl. Phys. Lett. **72**, 3199 (1998).
[15] R. A. Street, *Hydrogenated amorphous silicon* (Cambridge University Press, 1991).
[16] P. Schulz, E. Edri, S. Kirmayer, G. Hodes, D. Cahen, and A. Kahn, Energy Environ. Sci. **7**, 1377 (2014).
[17] R. Anthonj, N. Karl, B. E. Robertson, and J. J. Stezowski, J. Chem. Phys. **72**, 1244 (1980).
[18] K.-U. Ritzau, M. Bivour, S. Schröer, H. Steinkemper, P. Reinecke, F. Wagner, and M. Hermle, Sol. Energ. Mat. Sol. Cells **131**, 9 (2014).
[19] X. Liu, F. Wang, and Q. Wang, Phys. Chem. Chem. Phys. **14**, 7894 (2012).
[20] J. Brillet, J.-H. Yum, M. Cornuz, T. Hisatomi, R. Solarska, J. Augustynski, M. Graetzel, and K. Sivula, Nat. Photon. **6**, 824 (2012).
[21] M. T. Greiner, L. Chai, M. G. Helander, W.-M. Tang, and Z.-H. Lu, Adv. Funct. Mater. **22**, 4557 (2012).
[22] C.-Y. Lee, M. I. A. Aziz, S. Wenham, and B. Hoex, Jpn. J. Appl. Phys. **56**, 08MA08 (2017).
[23] M. Bivour, J. Temmler, H. Steinkemper, and M. Hermle, Sol. Energ. Mat. Sol. Cells **142**, 34 (2015).
[24] L. G. Gerling, S. Mahato, A. Morales-Vilches, G. Masmitja, P. Ortega, C. Voz, R. Alcubilla, and J. Puigdollers, Sol. Energ. Mat. Sol. Cells **145**, 109 (2015).
[25] C. Tao, S. Ruan, G. Xie, X. Kong, L. Shen, F. Meng, C. Liu, X. Zhang, W. Dong, and W. Chen, Appl. Phys. Lett. **94**, 43311 (2009).
[26] M. Mews, L. Korte, and B. Rech, Sol. Energ. Mat. Sol. Cells **158**, 77 (2016).
[27] M. Mews, A. Lemaire, and L. Korte, IEEE J. Photovolt. **7**, 1209 (2017).
[28] G. Oh, J. Jeon, K. S. Lee, and E. K. Kim, J. Nanosci. Nanotechnol. pp. 5109–5113 (2016).
[29] J. Yu, J. Zhou, J. Bian, L. Zhang, Y. Liu, J. Shi, F. Meng, J. Liu, and Z. Liu, Jpn. J. Appl. Phys. **56**, 08MB09 (2017).
[30] D.-J. Kim, B.-S. Kim, and H.-K. Kim, Thin Solid Films **547**, 225 (2013).
[31] A. Pan and T. P. Ma, Appl. Phys. Lett. **37**, 163 (1980).
[32] S. Li, Z. Yao, J. Zhou, R. Zhang, and H. Shen, Mater. lett. **195**, 213 (2017).
[33] A. A. Akl, H. Kamal, and K. Abdel-Hhady, Physica B **325**, 65 (2003).
[34] R. E. Agbenyeke, E. A. Jung, B. K. Park, T.-M. Chung, C. G. Kim, and J. H. Han, Appl. Surf. Sci. **419**, 758 (2017).
[35] R. Liu, Y. Lin, L.-Y. Chou, S. W. Sheehan, W. He, F. Zhang, H. J. M. Hou, and D. Wang, Angew. Chem. Int. Ed. **50**, 499 (2011).
[36] Z. S. Houweling, J. W. Geus, M. de Jong, P.-P. R. Harks, K. H. van der Werf, and R. E. Schropp, Mater. Chem. Phys. **131**, 375 (2011).
[37] J. Kane, H. Schweizer, and W. Kern, Thin Solid Films **29**, 155 (1975).
[38] P. Koscielniak, J. Mazur, J. Henek, M. Kwoka, L. Pawela, and J. Szuber, Thin Solid Films **520**, 927 (2011).
[39] P. L. R. J. Ip, T.P. Nguyen, Synth. Met **138**, 107 (2003).
[40] F. Bussolotti, L. Lozzi, M. Passacantando, S. L. Rosa, S. Santucci, and L. Ottaviano, Surf. Sci. **538**, 113 (2003).
[41] J.-S. Lee, I.-H. Jang, and N.-G. Park, J. Phys. Chem. C **116**, 13480 (2012).
[42] G. E. Jellison and F. A. Modine, Appl. Phys. Lett. **69**, 2137 (1996).
[43] S. D'Elia, N. Scaramuzza, F. Ciuchi, C. Versace, G. Strangi, and R. Bartolino, Appl. Surf. Sci. **255**, 7203 (2009).
[44] I. Valyukh, S. Green, H. Arwin, G. Niklasson, E. Wackelgard, and E. Granqvist, Sol. Energ. Mat. Sol. Cells **94**, 724 (2010).
[45] A. V. J. Tauc, R. Grigorovici, Phys. Stat. Sol. **15**, 627 (1966).
[46] H. R. Fallah, M. Ghasemi, A. Hassanzadeh, and H. Steki, Physica B **373**, 274 (2006).
[47] K. Heilig, Surf. Sci. **44**, 421 (1974).
[48] S. P. Harvey, T. O. Mason, Y. Gassenbauer, R. Schafranek, and A. Klein, J. Phys. D: Appl. Phys. **39**, 3959 (2006).
[49] M. Mews, M. Liebhaber, B. Rech, and L. Korte, Appl. Phys. Lett. **107**, 13902 (2015).
[50] F. Feldmann, M. Simon, M. Bivour, C. Reichel, M. Hermle, and S. W. Glunz, Sol. Energ. Mat. Sol. Cells **131**, 100 (2014).

[51]Z. Zhang and J. T. Yates, Chem. Rev. **112**, 5520 (2012).
[52]J. Frisch, A. Vollmer, J. Rabe, and N. Koch, Organic Electronics **12**, 916 (2011).
[53]D. C. Gleason-Rohrer, B. S. Brunschwig, and N. S. Lewis, J. Phys. Chem. C **117**, 18031 (2013).
[54]W. Mönch, *Electronic Properties of Semiconductor Interfaces* (Springer, 2004).
[55]L. G. Gerling, C. Voz, R. Alcubilla, and J. Puigdollers, J. Mater. Res. **32**, 260 (2017).
[56]J. P. Kleider, A. S. Gudovskikh, and P. R. i Cabarrocas, Appl. Phys. Lett. **92**, 162101 (2008).
[57]L. Korte, R. Rössler, and C. Pettenkofer, J. Appl. Phys. **115**, 203715 (2014).